

# Coarse molecular-dynamics analysis of an order-to-disorder transformation of a krypton monolayer on graphite

Miguel A. Amat,<sup>1</sup> Marco Arienti,<sup>2</sup> Vladimir A. Fonoberov,<sup>3</sup> Ioannis G. Kevrekidis,<sup>4</sup> and Dimitrios Maroudas<sup>1,a)</sup>

<sup>1</sup>Department of Chemical Engineering, University of Massachusetts Amherst, Amherst, Massachusetts 01003, USA

<sup>2</sup>United Technologies Research Center, 411 Silver Lane, East Hartford, Connecticut 06108, USA

<sup>3</sup>AIMdyn, Inc., 1919 State St., Suite 207, Santa Barbara, California 93101, USA

<sup>4</sup>Department of Chemical Engineering and Program in Applied and Computational Mathematics, Princeton University, Princeton, New Jersey 08544, USA

(Received 4 August 2008; accepted 2 October 2008; published online 11 November 2008)

The thermally induced order-to-disorder transition of a monolayer of krypton (Kr) atoms adsorbed on a graphite surface is studied based on a coarse molecular-dynamics (CMD) approach for the bracketing and location of the transition onset. A planar order parameter is identified as a coarse variable,  $\psi$ , that can describe the macroscopic state of the system. Implementation of the CMD method enables the construction of the underlying effective free-energy landscapes from which the transition temperature,  $T_t$ , is predicted. The CMD prediction of  $T_t$  is validated by comparison with predictions based on conventional molecular-dynamics (MD) techniques. The conventional MD computations include the temperature dependence of the planar order parameter, the specific heat, the Kr–Kr pair correlation function, the mean square displacement and corresponding diffusion coefficient, as well as the equilibrium probability distribution function of Kr-atom coordinates. Our findings suggest that the thermally induced order-to-disorder transition at the conditions examined in this study appears to be continuous. The CMD implementation provides substantial computational gains over conventional MD. © 2008 American Institute of Physics.

[DOI: 10.1063/1.3006427]

## I. INTRODUCTION

Physical adsorption (physisorption) refers to the weak binding of atoms and molecules to surfaces and is characterized by a low binding energy ( $\sim 0.3$  eV) of a single adatom. This phenomenon is commonly displayed by inert gases and saturated molecules. These adsorbate species are characterized by weak interactions and low cohesive energies when they form an adsorbate layer. Typical dynamics of such adsorbate layers on substrates at monolayer and submonolayer coverage is characterized by the motion of individual atoms or molecules along directions parallel to the surface; in the direction normal to the surface, the motion is restricted only to low-amplitude temperature-dependent oscillations. Even when these films undergo phase transitions, correlation lengths remain dominant along the two lateral directions, making this an effectively two-dimensional (2D) problem.<sup>1</sup> In contrast to bulk materials, these quasi-2D films form commensurate phases resulting from the influence of the underlying substrate. Due to the wide range of possible adsorbate-substrate combinations, the observed physical behavior is rich, as well as complex. Various atomistic models have been developed and implemented for the systematic and accurate prediction of such physical behavior.

The construction of reliable atomistic models that describe properly physical adsorption depends on the availabil-

ity of accurate descriptions of the corresponding interatomic forces. A thorough treatment of this subject is presented in the book by Bruch *et al.*<sup>1</sup> The main interactions involved in physisorption include adsorbate-adsorbate interatomic interactions, adsorbate-surface interactions, as well as the effects that the presence of the substrate imparts on the interatomic interactions. While a complete and rigorous description of all aspects of adsorption phenomena requires full knowledge of the corresponding electronic density distributions, as well as the response of adsorbed species to external fields, the range of applicability of this level of theory is limited severely due to the length scales required for studies of adsorbate layers (e.g., for disordered layers). Consequently, models for the study of physisorbed layers do not rely on quantum mechanical Hamiltonians to describe the underlying atomic-scale physics but on coarser descriptions (that do not involve explicitly the electronic degrees of freedom); these are developed either through *ab initio* theories or empirically, i.e., they constitute semiempirical or empirical models parametrized using experimental data.<sup>1</sup> This information is then used to construct interatomic potentials, which depend only on the positions of the atomic nuclei and are commonly used in classical models for molecular dynamics (MD).

The parametrization of such classical models or force fields takes into account three main interaction regimes: short-, intermediate-, and long-range. While the long- and short-range interactions are fairly well understood,<sup>1</sup> obtaining good descriptions of the intermediate-range interactions

<sup>a)</sup>Author to whom correspondence should be addressed. Electronic mail: maroudas@ecs.umass.edu.

remains a major challenge. Efforts aimed at illustrating how accurate potentials are constructed in order to describe properly the various interactions of inert gases commonly found in physisorption have been presented in the monograph by Klein<sup>2</sup> and in numerous articles by Aziz and co-workers.<sup>3–23</sup>

The problem becomes increasingly more complex when the interactions between inert gases and substrates are introduced. The studies by Steele<sup>24</sup> and Carlos and Cole<sup>25</sup> are representative of the efforts for constructing semiempirical models for such interactions and have served as the framework for a wide range of studies spanning a period of over 3 decades.<sup>24–42</sup> These studies<sup>24,25</sup> involve the construction of effective adsorbate-substrate holding potentials for substrates of graphite, which are typically based on pairwise (e.g., Lennard-Jones) potentials and the use of mixing rules and/or fits to experimental data in order to determine the parameters that describe the strength of the adsorbate-graphite interaction. Despite their relative simplicity, this class of potentials has been extremely successful in elucidating important aspects of physisorption phenomena, including phase transitions of physisorbed layers. Nevertheless, this type of models has remained deficient in describing the surface corrugation.<sup>29–35</sup> The first attempt to address such shortcomings theoretically was made by Carlos and Cole.<sup>25</sup> In their seminal work,<sup>25</sup> Carlos and Cole introduced noncentral pair potentials in order to incorporate the effects of the dielectric anisotropy of the graphite substrate on helium layers adsorbed on graphite. More recently, Shrimpton and Steele<sup>34</sup> presented a more empirical but effective approach that involves a scaling factor,  $s$ , intended to modify the corrugation-related term of the potential and to obtain the surface corrugation that yields the best agreement with experimental observations for krypton layers adsorbed on graphite.<sup>34,43,44</sup>

The work presented in this article features the development and implementation of a coarse molecular-dynamics (CMD) method for the prediction of the onset of thermally induced order-to-disorder and disorder-to-order transformations exhibited by inert gases adsorbed on graphite substrates. The CMD method is designed to function as a wrapper around an existing MD model based on a holding-potential form described previously.<sup>24,25,34</sup> This CMD method allows the extraction of the relevant macroscopic information associated with the thermally induced transition from the evolution of a properly chosen coarse variable. The method uses short bursts of MD runs that are judiciously initialized to map efficiently the important regions of the relevant coarse-variable space that describes the state of the system. The specific system chosen to illustrate the development and implementation of this CMD method consists of a monolayer of krypton (Kr) atoms physisorbed on a graphite substrate surface, which is known to undergo a thermally induced order-to-disorder transition at around 130 K.<sup>43,44</sup> The CMD-based prediction of this transition onset is validated by comparison with new original results obtained using conventional MD techniques.

The article is structured as follows. The description of the interaction potentials and the computational methods used in the MD simulations is given in Sec. II. The analysis

toward prediction of the thermally induced order-to-disorder transition onset for Kr monolayers physisorbed on graphite substrate surfaces according to conventional MD computations is presented in Sec. III. In Sec. IV, a CMD approach for predicting the transition onset is outlined and the CMD results are presented and discussed. Finally, the major conclusions of this study are summarized in Sec. V.

## II. MODEL DESCRIPTION FOR MOLECULAR-DYNAMICS SIMULATIONS

The model system employed in the MD simulations consists of a graphite substrate with a surface of dimensions  $127.8 \times 147.6 \text{ \AA}^2$  in the simulation supercell. A monolayer of Kr atoms is arranged initially in a  $(\sqrt{3} \times \sqrt{3})$  phase at the commensurate density,  $\rho_c$ , and placed at  $3.36 \text{ \AA}$  above the substrate surface. Periodic boundary conditions are imposed along the  $x$ - and  $y$ -directions (where the  $xy$ -plane is the plane of the surface), while the Kr atoms are free to move in the  $z$ -direction. The Kr–Kr interactions are described according to a 6–12 Lennard-Jones potential with the parameters  $\epsilon_{\text{Kr-Kr}}=170 \text{ K}$  and  $\sigma_{\text{Kr-Kr}}=3.60 \text{ \AA}$  found in Ref. 34. The potential is constructed to vanish smoothly and continuously at a distance  $r_c$  using cubic splines; this cutoff radius,  $r_c$ , is set at  $10.57 \text{ \AA}$ . The Kr-graphite (Kr-gr) interactions are described according to the effective potential,  $V(\mathbf{r})$ , of Shrimpton and Steele<sup>34</sup> with  $\epsilon_{\text{Kr-gr}}=75 \text{ K}$  and  $\sigma_{\text{Kr-gr}}=3.42 \text{ \AA}$ .

$$V(\mathbf{r}) = V_0(z) + s \sum_{\mathbf{G} \neq 0} V_{\mathbf{G}}(z) \exp(i\mathbf{G} \cdot \mathbf{R}), \quad (1)$$

where  $\mathbf{r}$  is the position vector of the Kr atom under consideration,  $V_0$  is the laterally averaged potential term, which depends on the height coordinate,  $z$ , of the Kr atom with respect to the graphite surface,  $\mathbf{G}$  refers to the corresponding reciprocal lattice vectors of the graphite surface, and  $\mathbf{R}$  is the 2D projection on the graphite surface of the position vector of the Kr atom,  $\mathbf{r}$ . The term  $V_{\mathbf{G}}(z)$  describes the corrugation of the graphite surface and  $s$  is the scaling factor for the modification of this corrugation-related term as discussed above. The  $V_0$  and  $V_{\mathbf{G}}$  terms, obtained using the isotropic 6–12 Lennard-Jones potential, are given by

$$V_0(z) = \frac{4\pi\epsilon\sigma^6}{a_s d^4} \left[ \frac{2}{5} \left( \frac{\sigma}{d} \right)^6 \zeta \left( 10, \frac{z}{d} \right) - \zeta \left( 4, \frac{z}{d} \right) \right] \quad (2)$$

and

$$V_{\mathbf{G}}(z) = \frac{\pi\epsilon\sigma^6\beta_{\mathbf{G}}}{a_s} \left( \frac{G}{2z} \right)^2 \left[ \left( \frac{\sigma^6}{15} \right) \left( \frac{G}{2z} \right)^3 K_5(Gz) - 4K_2(Gz) \right], \quad (3)$$

where  $a_s$  is the area of the unit cell in the basal plane of graphite and  $G$  is the magnitude of the reciprocal lattice vector  $\mathbf{G}=(01)$ . The factor  $\beta_{\mathbf{G}}$  is given by

$$\beta_{\mathbf{G}} = \exp(-i\mathbf{G} \cdot \mathbf{\Lambda}_1) + \exp(-i\mathbf{G} \cdot \mathbf{\Lambda}_2), \quad (4)$$

where  $\mathbf{\Lambda}_1$  and  $\mathbf{\Lambda}_2$  are the position vectors of the two carbon

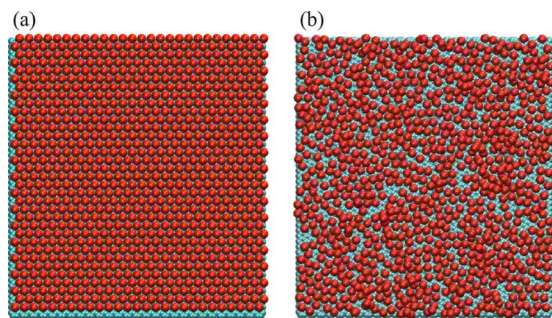


FIG. 1. (Color online) Snapshots of the atomic configurations of the krypton-on-graphite system at (a) low-temperature ( $T=30$  K),  $T < T_t$ , ordered and (b) high-temperature ( $T=150$  K),  $T > T_t$ , disordered states.

atoms in the planar unit cell. In Eq. (2),  $d$  is the interplanar spacing of graphite ( $d=3.37$  Å) and  $\zeta(n, x)$  is the  $n$ th-order Riemann-zeta function given by

$$\zeta(n, x) = \sum_{j=0}^{\infty} (j+x)^{-n}. \quad (5)$$

In Eq. (3),  $K_n(x)$  is the modified Bessel function of order  $n$  of the second kind. The functional form of this potential follows from the isotropic 6–12 potential of Carlos and Cole<sup>25</sup> with a factor  $s=1.5$  that was introduced in order to modify the corrugation of the potential required to reproduce a ground state consistent with the krypton-on-graphite experimental observations.<sup>34</sup>

In the MD simulations, the classical equations of motion were integrated in the canonical ensemble ( $NVT$ ) using the Nose–Hoover Chains algorithm<sup>45</sup> with a fine time step (1 fs). The cell-link method was used to facilitate the computation of the interatomic distances between Kr atoms and the  $z$ -dependent parts of the effective potential were computed using tabulated values<sup>34</sup> and cubic-spline interpolation. A rigid wall was placed at a distance of  $3r_c$  above the surface in order to contain in the simulation cell any Kr atoms that may stride off the surface layer. However, desorption of Kr atoms was found to be negligible at temperatures below and near the transition temperature. This was established by analysis of the mean-squared displacement (MSD) evolution both including and separately accounting for contributions due to lateral atomic displacements and atomic displacements normal to the surface plane.

### III. PREDICTION OF THE ORDER-TO-DISORDER TRANSFORMATION ONSET FOR KRYPTON LAYERS PHYSISORBED ON GRAPHITE

The krypton-on-graphite adsorbate-on-substrate system undergoes an order-to-disorder transition at a temperature,  $T_t$ , near 130 K.<sup>43,44</sup> Figure 1 shows atomic configurations of the system in the ordered [Fig. 1(a)] and disordered [Fig. 1(b)] states in the low-temperature limit and at  $T > T_t$ , respectively. In this section, two sampling schemes based on “conventional” MD methods are presented in order to monitor the atomic dynamics and predict this transition onset. In addition

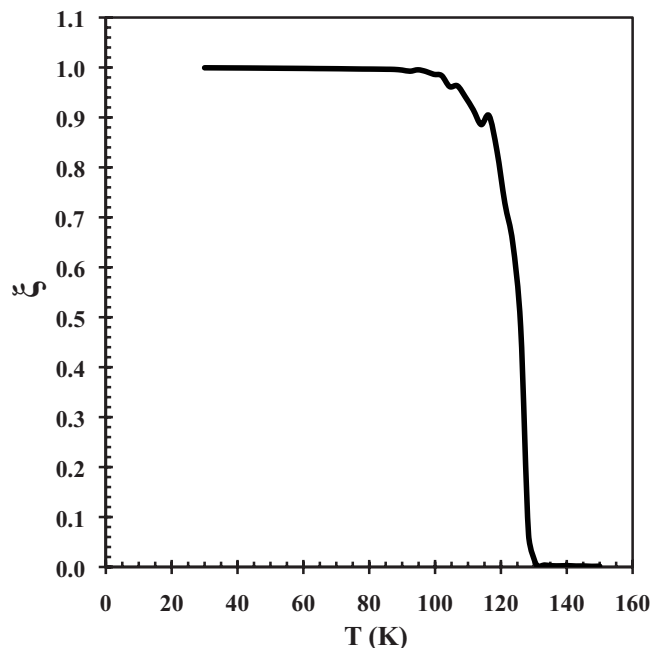


FIG. 2. Planar order parameter,  $\xi$ , as a function of temperature,  $T$ , for the krypton-on-graphite system. Upon heating, the system remains commensurate almost up to the transition onset, in agreement with experimental observations. The order-to-disorder transition occurs at  $T=126$  K.

to predicting the transition onset, the conventional MD results obtained will be used to validate the predictions of the CMD analysis presented in Sec. IV.

The first of these two conventional sampling schemes involves a heating schedule initialized with the system at its perfect ( $\sqrt{3} \times \sqrt{3}$ ) phase: the temperature is set to 30 K and the system is equilibrated for a period of 1 ns. The resulting atomic configuration at the end of this simulation run is used as the initial configuration for the next simulation run where the new temperature is raised by 2.4 K. This run-heat-run procedure is then repeated until the system reaches a temperature of 150 K, which is well above the expected transition onset,  $T_t$ , for the model potential employed. At each simulation run, two properties are computed: the “instantaneous” planar order parameter,  $\xi$ , of the quasi-2D Kr layer and its specific heat,  $C_V$ ;  $\xi$  is monitored during each run, while  $C_V$  is computed at the end of the run, using all the stored information for the energy evolution.

The planar order parameter,  $\xi$ , reveals important structural features and its variation with temperature provides important information regarding order-to-disorder or disorder-to-order transitions. It is defined by

$$\xi \equiv (1/N^2) \left| \sum_{j=1}^N \exp(i\mathbf{k} \cdot \mathbf{q}_j) \right|^2,$$

where  $\mathbf{q}_j$  is a 2D vector that corresponds to the position vector of the  $j$ th Kr atom projected onto the surface plane,  $\mathbf{k}$  is a reciprocal lattice vector of the reciprocal lattice associated with the Bravais lattice spanned by the ( $\sqrt{3} \times \sqrt{3}$ ) phase, and  $N$  is the number of Kr atoms in the computational supercell. Expressing  $\xi$  in terms of sines and cosines yields

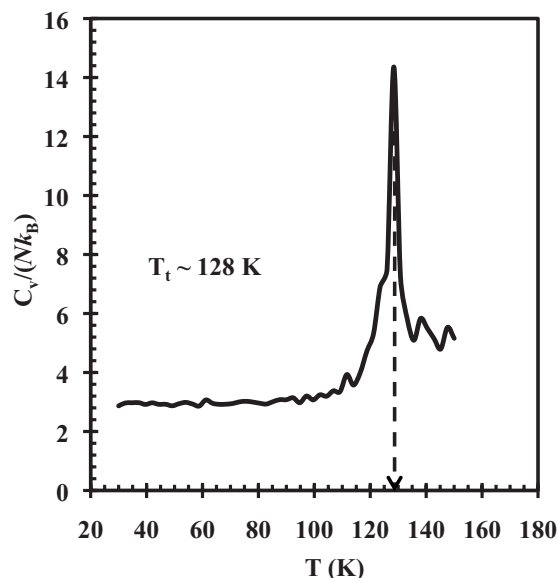


FIG. 3. Specific heat,  $C_V$ , as a function of temperature,  $T$ , for the krypton-graphite system obtained from fluctuations of the total energy. The temperature is ramped at 2.4 K increments. The sharp peak centered around  $T_t \cong 128$  K reveals the transition onset.

$$\xi = \left[ \frac{1}{N} \sum_{j=1}^N \cos(\mathbf{k} \cdot \mathbf{q}_j) \right]^2 + \left[ \frac{1}{N} \sum_{j=1}^N \sin(\mathbf{k} \cdot \mathbf{q}_j) \right]^2. \quad (6)$$

By definition, order-parameter values of  $\xi=1$  correspond to the perfect  $(\sqrt{3} \times \sqrt{3})$  phase, whereas order-parameter values of  $\xi=0$  correspond to phases other than the  $(\sqrt{3} \times \sqrt{3})$  phase. In the case of the thermally induced transition of the Kr-on-graphite system examined here, a value of  $\xi=0$  corresponds to the disordered phase.

The dynamics of inert-gas layers adsorbed on graphite is characterized by two clearly distinct time scales: a short scale involving the vibration of inert-gas atoms around the adsorption sites (ASs) and a longer scale involving jumps between available ASs. The vibrations around ASs are characterized by oscillations with temperature-dependent amplitudes. To filter out these vibrational effects in the calculation of the planar order parameter of the Kr layer,  $\mathbf{q}_j$  in Eq. (6) is replaced with  $\langle \mathbf{q}_j \rangle$ , where the brackets  $\langle \rangle$  indicate an average over the positions of the  $j$ th Kr atom over an observation time interval that includes several vibrational periods. It was found that an observation period of 40 ps was sufficiently long to obtain appropriate results (i.e., at temperatures below  $T_t$ , the calculated average is centered around an AS). The results shown in Fig. 2 reveal that the system remains commensurate (i.e., the values of  $\xi$  remain near 1) for temperatures up to the transition point, in agreement with experimental observations.<sup>43,44</sup> A sudden drop in the value of  $\xi$  marks the onset of the order-to-disorder transition. The transition onset is approximated by the temperature,  $T_t$ , at which the order parameter takes on a value of  $\xi=0.5$ ; the results of Fig. 2 yield  $T_t=126$  K.

The specific heat,  $C_V$ , was computed from the fluctuations of the total energy<sup>46</sup> to provide an additional, thermodynamic criterion for locating the onset of the thermally induced transition for the Kr-on-graphite system. As shown in

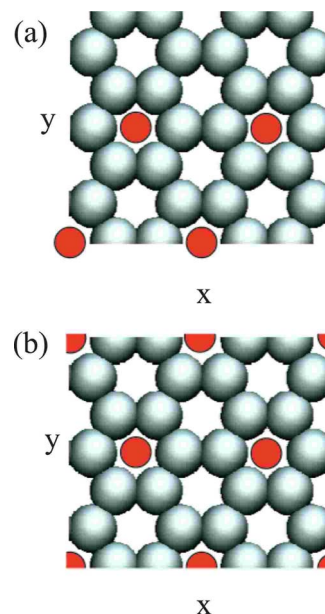


FIG. 4. (Color online) (a) Transformation of atomic coordinates to occupy reduced cell containing only four adsorption sites that fills 2D space if repeated periodically. (c) The reduced-space cell under the action of periodic boundary conditions.

Fig. 3, a peak centered at around  $T=128$  K marks the transition onset. The exhibited variation of the specific heat with temperature and the continuity of  $C_V(T)$  is representative of a second-order phase transition.

The second conventional MD method used to determine the transition onset involves an exhaustive ensemble sampling (ES) over a period of 4 ns. The Kr-on-graphite system is initialized from its commensurate  $(\sqrt{3} \times \sqrt{3})$  phase at temperatures over the range from 40 to 140 K. In this case, there is no heating schedule involved, and the temperatures are set to their target values directly. At each simulation run, three properties are computed: an equilibrium probability distribution function (PDF) of the particle (Kr-atom) coordinates, the MSD and the corresponding diffusion coefficient,  $D$ , and the Kr-Kr pair correlation function,  $g(r)$ .

The PDF is constructed by transforming (folding) the space occupied by all particles (Kr atoms) to that occupied by four *effective* particles at their  $(\sqrt{3} \times \sqrt{3})$  positions contained in the corresponding 2D supercell as shown in Fig. 4. In other words, all particles in the system are assigned a new set of “local” coordinates and are kept within this new cell by imposing the corresponding reduced-space periodic boundary conditions (rs-PBCs). The choice of four particles in this implementation has no particular significance and is made mainly for visual convenience. Monitoring these local coordinates enables the construction of the PDF, which is related visually to the state of the system (commensurate versus noncommensurate) at each temperature of interest.

When dealing with systems at the commensurate density,  $\rho_c$ , and at temperatures below the transition onset ( $T < T_t$ ), the PDF is expected to exhibit four peaks of equal height centered at the corresponding ASs and distributed among these four ASs of the reduced supercell. This behavior is evident in the distributions of Figs. 5(a) and 5(b) at temperatures of 125 and 126 K, respectively. The distributions of

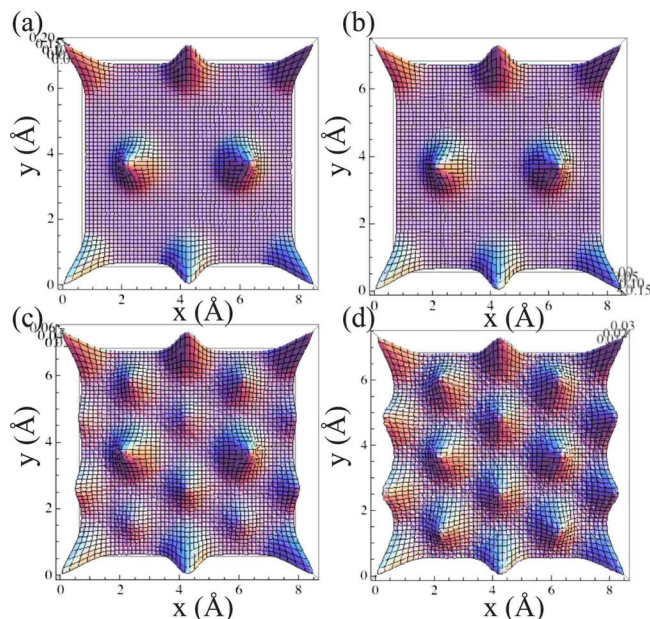


FIG. 5. (Color online) PDFs of the effective-particle coordinates for the Kr-on-graphite system obtained at (a) 125 K, (b) 126 K, (c) 127 K, and (d) 130 K. In (a) and (b), the shown PDFs are centered at the  $(\sqrt{3} \times \sqrt{3})$ -phase adsorption sites. Increasing the temperature from 126 to 127 K reveals a transition onset: the two PDFs shown in (c) and (d) indicate a finite probability for the Kr atoms to occupy all the graphitic adsorption sites, i.e., additional sites to the  $(\sqrt{3} \times \sqrt{3})$  ones.

Figs. 5(c) and 5(d) correspond to temperatures of 127 and 130 K. This PDF dependence on the system temperature reveals that from 126 to 127 K the character of the distribution changes drastically: the particles are no longer confined to their  $(\sqrt{3} \times \sqrt{3})$  phase adsorption sites and they can now be found with finite probability also at equivalent graphitic adsorption sites other than, and in addition to, the  $(\sqrt{3} \times \sqrt{3})$  ones. These results imply that the onset of the order-to-disorder transition occurs at a temperature between 126 and 127 K.

The calculation of the Kr-atom self-diffusion coefficient,  $D(T)$ , through the  $xy$ -based (i.e., planar according to the 2D projection of the Kr atomic positions) MSD analysis provides a more quantitative measure for locating the order-to-disorder transition onset. The results for the MSD evolution at various temperatures and the temperature dependence of  $D$  as an Arrhenius plot of  $\ln(D)$  versus  $1/T$  are shown in Figs. 6 and 7, respectively, over a temperature range from 120 to 130 K. In these figures, two different behaviors corresponding to two different states are evident: one at temperatures  $120 \text{ K} \leq T \leq 126 \text{ K}$  and another one at  $T \geq 127 \text{ K}$ . The linear fits shown in Fig. 7 confirm that  $D(T)$  follows an Arrhenius-type relation in both states, characterized by different slopes (activation energy barriers) that correspond to an ordered and a disordered phase, respectively. Analyses of the individual  $x$ -,  $y$ -, and  $z$ -based MSD evolution curves and the corresponding diffusion coefficients,  $D_x$ ,  $D_y$ , and  $D_z$ , at temperatures below and above but near the transition temperature,  $T_t$ , revealed that  $D_z \ll D_x$  and  $D_z \ll D_y$  by several orders of magnitude; this confirms that the exhibited behavior for the Kr-on-graphite system is indeed quasi-2D.

The pair correlation function,  $g(r)$ , expresses the prob-

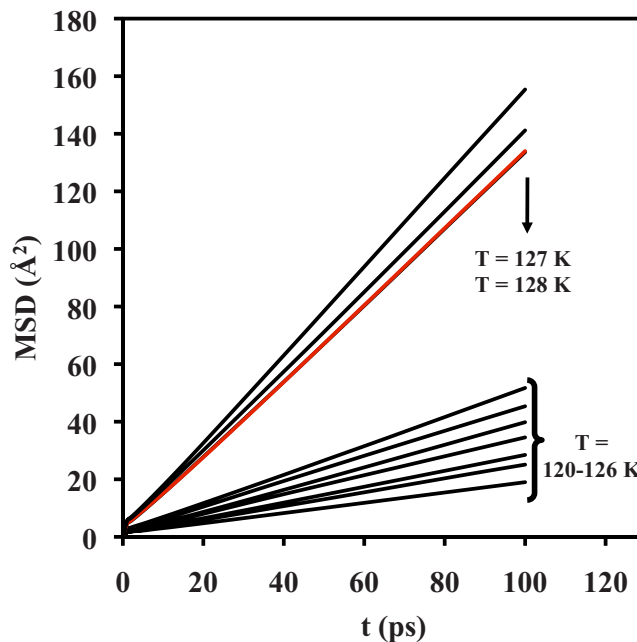


FIG. 6. (Color online) MSD evolution curves for various temperatures around the transition temperature,  $T_t$ . After an initial transient, the evolution curves become straight lines with slopes that reveal two different states corresponding to temperatures below ( $T \leq 126 \text{ K}$ ) and above ( $T \geq 127 \text{ K}$ ) the transition onset. The overlap between the evolution curves at  $T = 127$  and  $128 \text{ K}$  is attributed to the proximity of the former temperature to the transition onset. The red line is used to represent the MSD at  $T = 127 \text{ K}$ , which corresponds to the temperature that is closest to  $T_t$ .

ability of finding two atoms a distance  $r$  apart and contains important information about the structural state of the system, as characterized by the presence and/or absence of certain coordination shells. Pair correlation functions obtained at the end of constant-temperature runs over the range  $40 \text{ K} \leq T \leq 140 \text{ K}$  are shown in Fig. 8. To aid the visualiza-

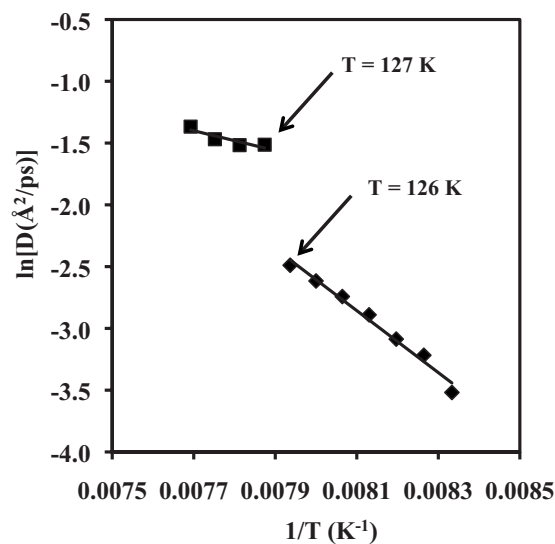


FIG. 7. Computed results and linear fits of  $\ln(D)$  as a function of  $1/T$ , i.e., an Arrhenius-type plot for the temperature dependence of the diffusion coefficient,  $D$ . The lower branch corresponds to the ordered (commensurate) state over the temperature range from 120 to 126 K. The upper branch corresponds to a second state, characterized by higher diffusion coefficients, for temperatures of 127 K and higher. This behavior confirms that the transition onset occurs at a temperature between 126 and 127 K.

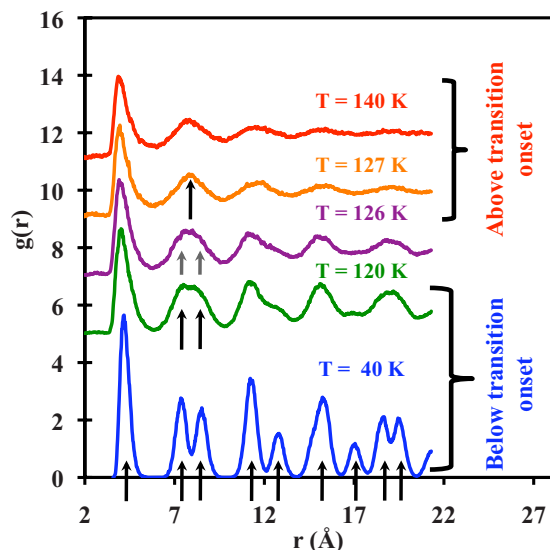


FIG. 8. (Color online) Pair correlation function profiles,  $g(r)$ , corresponding to temperatures of 40, 120, 126, 127, and 140 K. The profiles at  $T=120$ , 126, 127, and 140 K are shifted upwards by constant values of 5, 7, 9, and 11, respectively, for visual convenience. Solid arrows pointing to the peaks that indicate coordination shells characteristic of the  $(\sqrt{3} \times \sqrt{3})$  phase are shown in the  $g(r)$  corresponding to the lowest temperature. The braces are used to indicate temperatures below and above the transition onset,  $T_t$ , which correspond to states that are distinguished (most importantly) by the presence or absence of the third coordination shell. Traces from the third coordination shell can still be detected in the  $g(r)$  profile at 126 K; gray arrows are used to indicate the proximity to the transition onset.

tion, all the  $g(r)$  profiles are shifted by a constant value each except for the one at 40 K. Solid arrows pointing to peaks that indicate coordination shells characteristic of the  $(\sqrt{3} \times \sqrt{3})$  phase also are shown for the  $g(r)$  at 40 K. Detecting the second and third coordination shells at the various different temperatures allows one to distinguish between the ordered and disordered states found at temperatures between 40 and 120 K and above 127 K, respectively. The order-to-disorder transition is manifested most clearly by the disappearance of the third coordination shell, placing the location of the transition onset at a temperature between 126 and 127 K.

Finally, it should be mentioned that desorption and activation of Kr atoms change the actual coverage of the original monolayer; in our case, a very small fraction of Kr atoms was found in such a second layer with the first promoted atom being activated at  $T \sim 90$  K. This means that the actual surface coverage remains exactly equal to 1 up to  $T \sim 90$  K; at higher temperatures, the coverage decreases slightly and reaches a level of  $\sim 0.97$  at  $T = T_t$ , where the observed transition occurs. This implies that the transition onset calculated in this work may be in the vicinity of a triple state in the phase diagram and motivates the construction of the phase diagram in future work. In this context, it should also be pointed out that at a temperature  $T \sim 90$  K, the temperature dependencies of the order parameter,  $\xi$ , and the specific heat,  $C_V$ , Figs. 2 and 3, respectively, start deviating from the perfectly uniform behavior that corresponds to the ordered state.

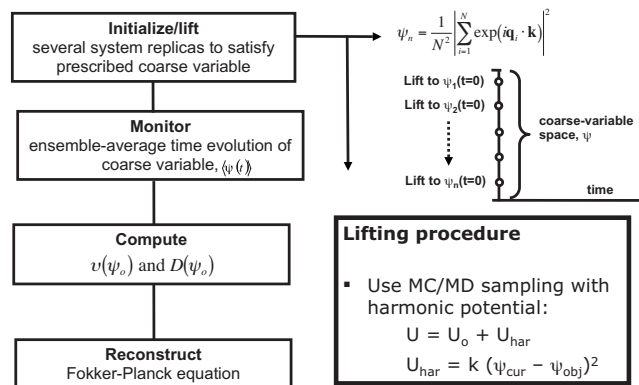


FIG. 9. Schematic outline of the CMD procedure implemented with emphasis on the *lifting* scheme for studying order-to-disorder transitions in the Kr-on-graphite system. The coarse-variable space,  $0 \leq \psi \leq 1$ , is mapped by implementing a MC-based sampling scheme with a quadratic penalty function (harmonic potential) that uses the current and target values of the coarse variable. Following this initialization, the constraint is released and the ensemble averaged coarse-variable evolution,  $\langle \psi(t) \rangle$ , is monitored to obtain the drift velocity,  $v(\psi_n)$ , and the diffusion coefficient,  $D(\psi_n)$ , of the underlying Fokker-Planck equation.

#### IV. CMD PREDICTION OF THE THERMALLY INDUCED ORDER-TO-DISORDER TRANSITION ONSET OF THE KR-ON-GRAPHITE SYSTEM

In this section, a CMD method is implemented to analyze the thermally induced order-to-disorder and disorder-to-order transformations exhibited by the Kr-on-graphite system. The CMD approach has been presented elsewhere.<sup>47–50</sup>

In brief, given the choice of an appropriate coarse variable  $\psi$  that describes properly the state of the system, CMD allows for (i) effective mapping of the coarse-variable space, (ii) on-the-fly extraction of the relevant macroscopic information, (iii) reconstruction of the underlying effective free-energy landscapes, and (iv) determination of the relevant transformation onset ( $T_t$  in the case of the thermally induced transition studied here), through the use of short MD simulation bursts. The CMD procedure that we implemented in this study is outlined in Fig. 9. The order parameter  $\xi$ , as defined in Eq. (6), is chosen as the relevant coarse variable,  $\psi \equiv \xi$ , for usefully describing the state of the system (i.e., commensurate/ordered versus noncommensurate/disordered). This coarse variable is then initialized *at will* to map its entire space  $\psi \in [0, 1]$  at increments of  $\Delta\psi = 0.05$ . This initialization is achieved by using a Metropolis-Monte-Carlo-based scheme with a quadratic penalty function (a harmonic potential) that takes into account the difference between the running and target values of the coarse variable,  $\psi$  and  $\psi_0$ , respectively, using a stiff and variable spring constant,  $K$ , initialized at  $K = 500$  (in reduced units) as illustrated in Fig. 9. The variation in the value of  $K$  is introduced by dividing its constant value by  $|\Delta\psi_n - \Delta\psi_c| + \delta$ , where  $\Delta\psi_n = (\psi_n - \psi_{obj})^2$ ,  $\Delta\psi_c = (\psi_c - \psi_{obj})^2$ , and  $\delta$  is a small value ( $\sim 10^{-5}$ ). The subscripts  $n$ ,  $c$ , and  $obj$  refer to the newly MC-generated trial value of the coarse variable, its previous value before the trial move, and its objective value, respectively. Once the target coarse-variable value,  $\psi_0$ , is satisfied, the system is equilibrated at this new state. Each sampled point in the coarse-variable space is comprised of an en-

semble of replicas and is represented by  $\langle\psi_0\rangle=\langle\psi(t=0)\rangle$ . Here, the brackets  $\langle\rangle$  indicate an ensemble average over 25 independent replicas of the system. Following this initialization (*lifting*) procedure, all constraints are released and the system is allowed to evolve using conventional MD (i.e., through a short burst of the atomistic time stepper). The averaged coarse-variable evolution,  $\langle\psi(t)\rangle$ , is then monitored over a time horizon of 200 ps, from which the drift velocity,  $v(\psi_0)$ , and diffusion coefficient,  $D(\psi_0)$ , are obtained and used to reconstruct the underlying Fokker–Planck equation. At temperatures near the transition onset, simulation runs of 200 ps are considered to be quite short with respect to the long-time coarse-variable evolution. This “short” time assessment is supported by the results shown in Figs. 6 and 7. Specifically, the overlap in the values of MSD and  $\ln(D)$  at temperatures of 127 and 128 K (i.e.,  $T\sim T_t$ ) in Figs. 6 and 7, respectively, reveals that a simulation period of 4 ns was not sufficiently long to distinguish between these two diffusion coefficient values due to the critical slowdown near the transition onset. The choice of the planar order parameter as the coarse variable at temperatures equal to or higher than 90 K, where a small fraction of Kr atoms is promoted over the first physisorbed layer, could affect the overall quality of the coarse variable; it is clear, however, that this coarse variable choice remains sufficient for describing the state of the system.

Representative coarse-variable evolution plots after releasing the *lifting* constraints are shown in Fig. 10. Figure 10(a) shows coarse trajectories,  $\langle\psi(t)\rangle$ , initiated at different  $\psi_0$  values at a temperature of 100 K, which is well below the transition temperature,  $T_t$ . It is evident that the system evolves toward the ordered state, which is represented by high values of the coarse variable, ( $\psi\cong 1$ ). Conversely, Fig. 10(b) shows representative coarse trajectories at a temperature that is well above  $T_t$ ,  $T=130$  K. In this case, the tendency of the coarse-variable evolution is toward the disordered state, which is represented by low values of the coarse variable, ( $\psi\cong 0$ ). This qualitative analysis of the coarse variable serves as a quick tool to bracket the location of the transition onset to within a narrower temperature range. Generation of at-will-initiated coarse trajectories at temperatures between 115 and 130 K along with the corresponding monitoring and analysis required to obtain the drift velocity,  $v(\psi_0)$ , and diffusion coefficient,  $D(\psi_0)$ , and the integration of the equilibrium version of the underlying Fokker–Planck equation in  $\psi$  allows for the reconstruction of the corresponding underlying effective free-energy landscapes. These landscapes,  $\Delta G/k_B T$  as a function of  $\psi$ , are shown in Fig. 11 over the temperature range of interest.

The coarse-variable definition stems from the assumption that the state of the system at temperatures well below and above the transition temperature,  $T_t$ , is represented by a one-dimensional free-energy landscape,  $\Delta G(\psi)/k_B T$ , consisting of two (half) wells that are centered at coarse-variable values of one and zero and correspond to the ordered (commensurate) and the disordered (noncommensurate) states, respectively. This trend is illustrated in Fig. 11, where the lowest and highest temperatures examined are 115 and 130 K, respectively. The broken dashed lines depict the bottoms of

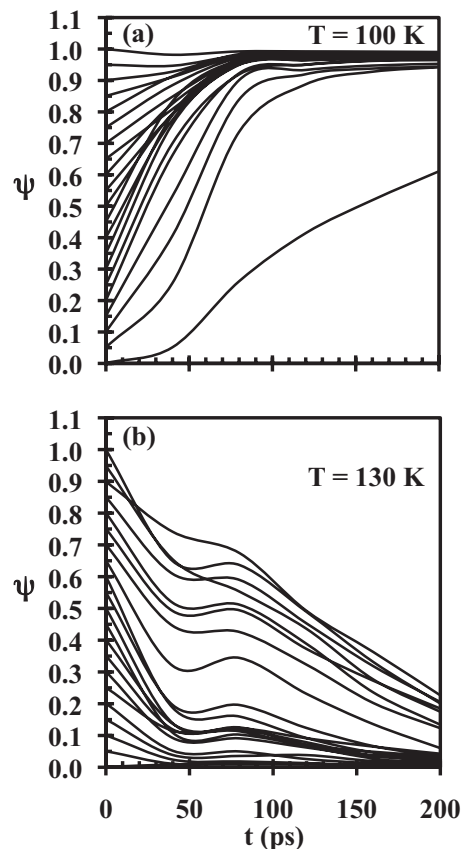


FIG. 10. Ensemble averaged coarse-variable evolution,  $\langle\psi(t)\rangle$ , after *lifting* at a temperature (a) well below ( $T=100$  K) and (b) well above ( $T=130$  K) the transition temperature,  $T_t$ . The coarse trajectories in (a) show that the system evolves to its ordered state ( $\psi\rightarrow 1$ ), while those in (b) show that the coarse evolution drifts toward the disordered state ( $\psi\rightarrow 0$ ). The observed crossing between some of the curves in the coarse-variable evolution may imply that a second coarse variable becomes important. This issue could be due to the small fraction of atoms promoted away from the original monolayer and is currently being investigated.

the effective free-energy wells corresponding to the ordered and disordered states, respectively. As shown in Fig. 11, the location of the effective free-energy well corresponding to the ordered state ( $0.5 < \psi \leq 1$ ) becomes shallower and shifts toward lower values of  $\psi$  as the temperature is increased. At temperatures  $T \geq 127.5$  K, a drastic change is observed resulting in effective free-energy wells that are now centered at  $\psi=0$ . Guided by this observation, the various effective free-energy landscapes can be assigned into one of two regions: a region at temperatures between 115 and 125 K corresponding to ordered states and designated by the downward pointing solid vertical line, and a region at temperatures  $T \geq 127.5$  K corresponding to the disordered state and designated by the upward pointing solid vertical line. It is important to note that the shape of the effective free-energy landscapes corresponds to either the solid or the melt phase as expected from a second-order transition.

Analysis of the effective free-energy landscapes at coarse-variable values near zero allows for calculation of the slope of  $\Delta G/k_B T$  with respect to  $\psi$  at each temperature studied. This slope calculation is illustrated in the inset to Fig. 12, where negative and positive slope values are related to the presence and absence of ordered states, respectively.

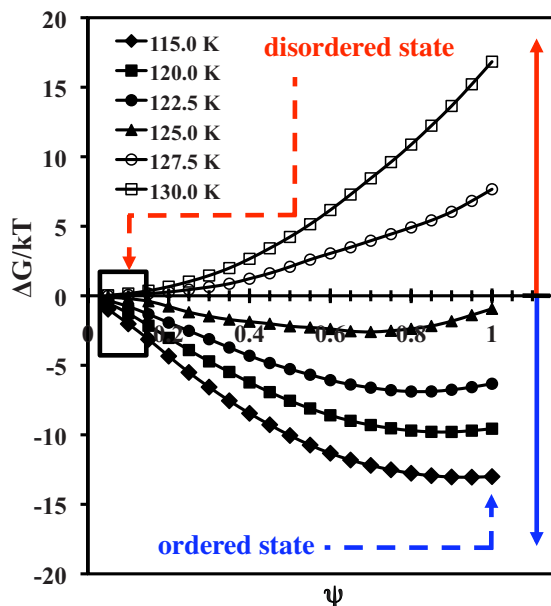


FIG. 11. (Color online) Effective free-energy landscapes for temperatures over the range  $115 \text{ K} \leq T \leq 130 \text{ K}$ . The broken dashed lines point to the bottom of the thermodynamic potential wells corresponding to the ordered and disordered states, respectively. The solid vertical lines are used to designate the regions corresponding to the ordered and disordered states, respectively. The square box shown encloses the region used to calculate the slopes that have been employed in the determination of the transition temperature,  $T_t$ .

These slope values,  $\Delta(\Delta G/k_B T)/\Delta\psi$ , are then plotted as a function of temperature and are shown in Fig. 12. The two regions above and below the transition onset are characterized by positive and negative slope values, respectively, and are represented by broken dashed and solid lines. Such ordered-disordered to negative-positive correspondence between the state of the system and the slope of the effective free-energy surface with respect to  $\psi$  allows for determining the transition onset in the limiting case where the slope becomes equal to zero. This is obtained by interpolation and yields a temperature of 126 K for the commensurate-to-fluid (order-to-disorder) transition for the Kr-on-graphite system. This criterion is based on thermodynamic arguments and yields results, which are in excellent agreement with the conventional MD-based results of Sec. III. Alternatively, the transition onset could be located by implementing a Newton-Raphson iterative procedure in “variable and parameter” space as has been shown elsewhere.<sup>51</sup>

## V. CONCLUSIONS

In conclusion, CMD has been validated as a technique that allows for the efficient bracketing and accurate location of the onset of the thermally induced order-to-disorder transition of krypton monolayers adsorbed on graphite. This assessment is based on the excellent agreement of the CMD prediction of the transition temperature,  $T_t$ , with that obtained using conventional MD techniques; these MD techniques were used to compute as a function of temperature the planar order parameter, specific heat, equilibrium probability distribution function of Kr-atom coordinates, mean-square displacement evolution and corresponding diffusion coeffi-

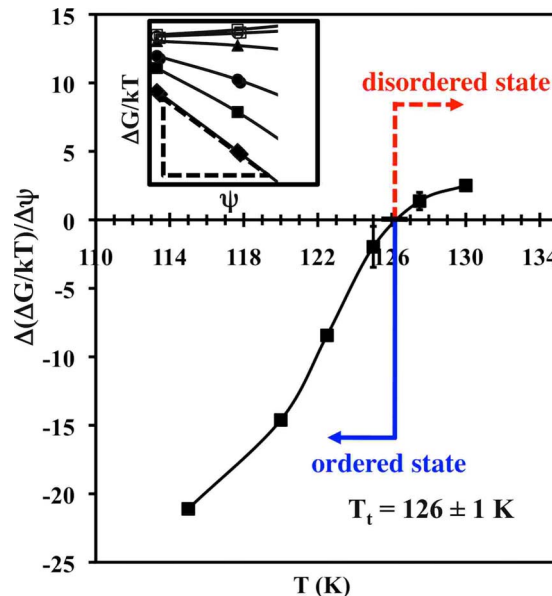


FIG. 12. (Color online) Temperature dependence of the slope of the effective free energy,  $\Delta(\Delta G/k_B T)/\Delta\psi$ , with respect to the coarse variable,  $\psi$ , used for the bracketing and determination of the transition onset,  $T_t$ . The inset corresponds to the box shown in Fig. 11 and is used to highlight the slope computation.

cient, and the Kr–Kr pair correlation function. CMD relies on the identification of a coarse variable,  $\psi$ , that describes properly the state of the system; it was shown that the planar order parameter,  $\xi$ , of Eq. (6) met this criterion successfully. Generation of short MD simulation bursts of ensembles of independent system replicas that satisfy chosen initial values of the coarse variable allowed for an efficient mapping of the entire coarse-variable space. This initialization at will achieved through implementation of the *lifting* scheme of Sec. IV and Fig. 9 presents a major advantage with respect to other techniques. Specifically, it bypasses problems associated with the sampling of states separated by high-energy barriers and allows for the sampling of regions of coarse-variable space that would otherwise be inaccessible. Furthermore, the capability that CMD offers to work very near the transition onset through short MD simulation bursts results in significant reduction in the computational overhead and bypasses many of the problems that are encountered with other conventional techniques near a transition onset, such as critical slowdown.

In this particular application, we found that CMD provided a boost factor of  $\sim 5$  in computational performance. This performance assessment was made with respect to the more accurate conventional MD results based on sampling through the 4-ns-long trajectories. However, it is emphasized that the overlap between the MSD evolution curves corresponding to the temperatures of 127 and 128 K shown in Fig. 6 is a clear indication that the 4 ns period was not entirely sufficient: longer runs together with larger system sizes should be employed to obtain more accurate measures for the “conventional” prediction of the transition temperature, which should result in larger computational gains for CMD. Finally, it should be mentioned that the many-replica struc-

ture of CMD is inherently well suited for “embarrassingly parallel” algorithm implementation that may provide even further computational advantages.

## ACKNOWLEDGMENTS

This work was supported by the National Science Foundation through Grant Nos. CTS-0205584, ECS-0317345, CTS-0417770, and CBET-0613501 (M.A.A. and D.M.) and by the U.S. DOE through CMPD and DARPA (I.G.K.). The work of M.A. and V.A.F. was funded by DARPA DSO (Cindy Daniell, PM) managed by the AFOSR Computational Mathematics Program (Fariba Fahroo, PM) under Robust Uncertainty Management Contract No. FA9550-07-C-0024. Useful discussions with G. Hummer and S. M. Auerbach are gratefully acknowledged. The DyNARUM team at United Technologies Research Center also is acknowledged for introducing us to the Kr-on-graphite problem.

- <sup>1</sup>L. W. Bruch, M. W. Cole, and E. Zaremba, *Physical Adsorption: Forces and Phenomena* (Oxford Science, New York, 1997).
- <sup>2</sup>M. L. Klein, *Inert Gases: Potentials, Dynamics, and Energy Transfer in Doped Crystals* (Springer-Verlag, Berlin, 1984).
- <sup>3</sup>H. J. Achtermann, J. G. Hong, G. Magnus, R. A. Aziz, and M. J. Slaman, *J. Chem. Phys.* **98**, 2308 (1993).
- <sup>4</sup>K. M. Smith, A. M. Rulis, G. Scoles, R. A. Aziz, and G. Duquette, *J. Chem. Phys.* **63**, 2250 (1975).
- <sup>5</sup>K. M. Smith, A. M. Rulis, G. Scoles, R. A. Aziz, and V. Nain, *J. Chem. Phys.* **67**, 152 (1977).
- <sup>6</sup>R. A. Aziz and H. H. Chen, *J. Chem. Phys.* **67**, 5719 (1977).
- <sup>7</sup>R. A. Aziz, *Int. J. Thermophys.* **8**, 193 (1987).
- <sup>8</sup>R. A. Aziz and A. R. Janzen, *Metrologia* **25**, 57 (1988).
- <sup>9</sup>R. A. Aziz, V. P. S. Nain, J. S. Carley, W. L. Taylor, and G. T. McConville, *J. Chem. Phys.* **70**, 4330 (1979).
- <sup>10</sup>R. A. Aziz, J. Presley, U. Buck, and J. Schleusener, *J. Chem. Phys.* **70**, 4737 (1979).
- <sup>11</sup>R. A. Aziz, P. W. Riley, U. Buck, G. Maneke, J. Schleusener, G. Scoles, and U. Valbusa, *J. Chem. Phys.* **71**, 2637 (1979).
- <sup>12</sup>R. A. Aziz, W. J. Meath, and A. R. Allnatt, *Chem. Phys.* **78**, 295 (1983).
- <sup>13</sup>R. A. Aziz and A. Van Dalen, *J. Chem. Phys.* **78**, 2402 (1983).
- <sup>14</sup>R. A. Aziz and A. Van Dalen, *J. Chem. Phys.* **78**, 2413 (1983).
- <sup>15</sup>W. J. Meath and R. A. Aziz, *Mol. Phys.* **52**, 225 (1984).
- <sup>16</sup>R. A. Aziz, A. Krantz, and M. J. Slaman, *Z. Phys. D: At., Mol. Clusters* **21**, 251 (1991).
- <sup>17</sup>M. J. Slaman and R. A. Aziz, *Int. J. Thermophys.* **12**, 837 (1991).
- <sup>18</sup>R. A. Aziz and M. J. Slaman, *Z. Phys. D: At., Mol. Clusters* **25**, 343 (1993).
- <sup>19</sup>R. A. Aziz, M. J. Slaman, and A. R. Janzen, *Phys. Rev. E* **49**, 5310 (1994).
- <sup>20</sup>A. R. Janzen and R. A. Aziz, *J. Chem. Phys.* **103**, 9626 (1995).
- <sup>21</sup>M. J. Slaman and R. A. Aziz, *Int. J. Thermophys.* **16**, 1029 (1995).
- <sup>22</sup>A. R. Janzen and R. A. Aziz, *J. Chem. Phys.* **107**, 914 (1997).
- <sup>23</sup>A. K. Dham, A. R. Allnatt, W. J. Meath, and R. A. Aziz, *Mol. Phys.* **67**, 1291 (1989).
- <sup>24</sup>W. A. Steele, *Surf. Sci.* **36**, 317 (1973).
- <sup>25</sup>W. E. Carlos and M. W. Cole, *Surf. Sci.* **91**, 339 (1980).
- <sup>26</sup>F. F. Abraham, S. W. Koch, and W. E. Rudge, *Phys. Rev. Lett.* **49**, 1830 (1982).
- <sup>27</sup>S. W. Koch and F. F. Abraham, *Phys. Rev. B* **27**, 2964 (1983).
- <sup>28</sup>F. F. Abraham, W. E. Rudge, D. J. Auerbach, and S. W. Koch, *Phys. Rev. Lett.* **52**, 445 (1984).
- <sup>29</sup>G. Vidali and M. W. Cole, *Phys. Rev. B* **29**, 6736 (1984).
- <sup>30</sup>M. Schöbinger and F. F. Abraham, *Phys. Rev. B* **31**, 4590 (1985).
- <sup>31</sup>S. W. Koch and F. F. Abraham, *Phys. Rev. B* **33**, 5884 (1986).
- <sup>32</sup>H. Y. Kim and M. W. Cole, *Phys. Rev. B* **35**, 3990 (1987).
- <sup>33</sup>T. M. Hakim, H. R. Glyde, and S. T. Chui, *Phys. Rev. B* **37**, 974 (1988).
- <sup>34</sup>N. D. Shrimpton and W. A. Steele, *Phys. Rev. B* **44**, 3297 (1991).
- <sup>35</sup>H. Y. Kim and W. A. Steele, *Phys. Rev. B* **45**, 6226 (1992).
- <sup>36</sup>W. A. Steele, *Chem. Rev. (Washington, D.C.)* **93**, 2355 (1993).
- <sup>37</sup>J. M. Houlrik, D. P. Landau, and S. J. Knak Jensen, *Phys. Rev. E* **50**, 2007 (1994).
- <sup>38</sup>F. Y. Hansen and L. W. Bruch, *Phys. Rev. B* **51**, 2515 (1995).
- <sup>39</sup>M. W. Roth, *Phys. Rev. B* **51**, 7778 (1995).
- <sup>40</sup>M. E. Pierce and E. Manousakis, *Phys. Rev. B* **62**, 5228 (2000).
- <sup>41</sup>K. E. Becker and K. A. Fichthorn, *J. Chem. Phys.* **125**, 184706 (2006).
- <sup>42</sup>A. D. Lueking and M. W. Cole, *Phys. Rev. B* **75**, 195425 (2007).
- <sup>43</sup>D. M. Butler, J. A. Litzinger, and G. A. Stewart, *Phys. Rev. Lett.* **44**, 466 (1980).
- <sup>44</sup>E. D. Specht, A. Mak, C. Peters, M. Sutton, R. J. Birgeneau, K. L. D'Amico, D. E. Moncton, S. E. Nagler, and P. M. Horn, *Z. Phys. B: Condens. Matter* **69**, 347 (1987).
- <sup>45</sup>G. J. Martyna, M. L. Klein, and M. Tuckerman, *J. Chem. Phys.* **97**, 2635 (1992).
- <sup>46</sup>D. C. Rapaport, *The Art of Molecular Dynamics Simulation* (Cambridge University Press, Cambridge, 2004).
- <sup>47</sup>G. Hummer and I. G. Kevrekidis, *J. Chem. Phys.* **118**, 10762 (2003).
- <sup>48</sup>D. I. Kopelevich, A. Z. Panagiotopoulos, and I. G. Kevrekidis, *J. Chem. Phys.* **122**, 044907 (2005); D. I. Kopelevich, A. Z. Panagiotopoulos, and I. G. Kevrekidis, *J. Chem. Phys.* **122**, 044908 (2005).
- <sup>49</sup>M. A. Amat, I. G. Kevrekidis, and D. Maroudas, *Phys. Rev. B* **74**, 132201 (2006).
- <sup>50</sup>M. A. Amat, I. G. Kevrekidis, and D. Maroudas, *Appl. Phys. Lett.* **90**, 171910 (2007).
- <sup>51</sup>S. Sriraman, I. G. Kevrekidis, and G. Hummer, *Phys. Rev. Lett.* **95**, 130603 (2005).